Journal of Biomedical Optics

SPIEDigitalLibrary.org/jbo

Concentration dependence of optical clearing on the enhancement of laser-scanning optical-resolution photoacoustic microscopy imaging

Qingliang Zhao
Lin Li
Qian Li
Xia Jiang
Qiushi Ren
Xinyu Chai
Chuanqing Zhou

SPIE

Concentration dependence of optical clearing on the enhancement of laser-scanning optical-resolution photoacoustic microscopy imaging

Qingliang Zhao,[a,†] Lin Li,[a,†] Qian Li,[a] Xia Jiang,[a] Qiushi Ren,[b] Xinyu Chai,[a,*] and Chuanqing Zhou[a,*]
[a]Shanghai Jiao Tong University, School of Biomedical Engineering, No. 800 Dongchuan Road, Shanghai 200240, China
[b]Peking University, College of Engineering, Department of Biomedical Engineering, Beijing 100871, China

Abstract. Quantitative analysis of optical clearing effects (OCE) induced by hyperosmotic agents is very important to optical tissue clearing applications in biomedical diagnostic imaging and therapeutics. This study aims at investigating the effect of glycerol concentration on the laser-scanning optical-resolution photoacoustic microscopy (LSOR-PAM) imaging contrast and light penetration depth. The photoacoustic (PA) signal amplitude changes are evaluated as a function of the concentration of glycerol. The results reveal that the PA signal amplitudes are enhanced with the glycerol concentration increasing, and also show that higher concentration of glycerol produces better light penetration and OCE on a phantom. The PA signal amplitude increases only 8.1% for 20% glycerol, but for higher concentrations, the increases are 76% and 165% for 40% and 60% glycerol, respectively. This preliminary study demonstrates that application of glycerol as an optical contrast agent reduces the tissue scattering and is beneficial to PAM imaging and optical diagnosis in clinical dermatology. © *2014 Society of Photo-Optical Instrumentation Engineers (SPIE)* [DOI: 10.1117/1.JBO.19.3.036019]

Keywords: photoacoustic imaging; concentration; glycerol; tissue; optical clearing; imaging through turbid media.

Paper 130823RR received Nov. 19, 2013; revised manuscript received Feb. 17, 2014; accepted for publication Feb. 18, 2014; published online Mar. 26, 2014.

1 Introduction

Photoacoustic microscopy (PAM) has been demonstrated as an advanced biological or biomedical imaging technique capable of detecting the physiological specific endogenous chromophores based on the optical absorption properties of the investigated target.[1–3] This imaging modality utilizes the acoustic wave generated by the laser-induced thermal–elastic expansion of the target to construct an image. Based on its focusing mechanism, two types of PAM have been developed: acoustic-resolution PAM and optical-resolution PAM (OR-PAM).[4,5] In OR-PAM, the lateral resolution primarily depends on the optical focal spot size and the axial resolution is determined by the ultrasonic transducer. Nevertheless, in strong scattering tissue such as skin, breast, bioliquids, etc., the optical focusing capability degrades due to optical scattering. Meanwhile, in the visible and near infrared (NIR) wavelengths, scattering in tissues is higher than the absorption. In addition, the imaging depth of OR-PAM is limited by the optical transport mean free path and affected by both photon absorption and scattering.[6,7] In order to overcome these challenges, various physical and chemical methods have been deployed to enhance photoacoustic (PA) imaging depth, PA signal-to-noise ratio and imaging resolution such as careful choosing of the excitation laser wavelength and utilization of optical contrast agents (OCAs).[7,8–10]

In recent years, the optical tissue clearing (OTC) technique has shown great potential in inducing optical clearing effects (OCEs) to reduce scattering in tissues using hyperosmotic and biocompatible chemicals agents.[11–14] The OCE induced by using OCA and the mechanisms of optical clearing (OC) are also discussed.[15–20] Recently, numerous investigations on OCA introduced effective OCAs, such as glucose solutions, dimethyl sulfoxide solution, glycerol, propylene glycol, etc., which have refractive index close to that of collagen and are applicable to alter the scattering properties of tissues.[11,12,21–24] Studies done by Ku and Wang[8] and Wang et al.[9] demonstrated that the application of OCA into chicken breast muscle and animal brains can significantly reduce light scattering and thereby enhance the resolution and imaging depth of photoacoustic tomography (PAT). Liu et al.[25] also proved that biocompatible and rapid OC of skin can minimize light scattering and thus increase optical resolution and sensitivity of PA flow cytometry.

Among all the PA imaging technologies, laser-scanning optical-resolution photoacoustic microscopy (LSOR-PAM) is a relatively new one for imaging biological tissue at a microscopic scale. It has demonstrated capabilities to improve scanning speed using two-dimensional galvanometer[26] and perform approximately real-time microscopic scale three-dimensional imaging of biological tissues.[27–29] The contrast and depth of this imaging technology is still limited as they are based on the laser focusing capability, which degrades due to the high scattering of tissue as mentioned above. Glycerol is one of the most common and efficient OCA in skin OC *in vitro* and *in vivo*,[30,31] and it has been proved in medical applications such as tooth therapy and cosmetics study.[32]

The OTC methods use high-refractive OCA mainly in order to reduce light scattering and thus enhance the light penetration

*Address all correspondence to: Chuanqing Zhou, E-mail: zhoucq@sjtu.edu.cn; Xinyu Chai, E-mail: xychai@sjtu.edu.cn

†The authors contributed equally to this work.

0091-3286/2014/$25.00 © 2014 SPIE

depth in tissue. Although, a lot of research has been done to assess the OTC efficacy by various optical methods such as NIR reflectance spectroscopy and optical coherence tomography (OCT), none of the studies has investigated OCE with different quantities of OCA on LSOR-PAM imaging method. Meanwhile, optimum concentration of OCA is important in such applications as a low concentration would not generate sufficient OCE and a high concentration would damage the biological tissues, even obstruct the blood vessel or cause the blood flow to stop.[33,34] In this study, we demonstrate that both the imaging visibility and PA signals amplitude of LSOR-PAM can be enhanced by using glycerol–water solution of different concentrations, which is one of the most efficient used OCA for biomedical imaging.

2 Materials and Methods

2.1 *LSOR-PAM System*

The schematic of our experimental LSOR-PAM system is shown in Fig. 1. A pulsed Nd:YAG laser (SPOT-10-100-532, Elforlight, Northampton, United Kingdom; Pulse width <1.8 ns) with a 532-nm wavelength and a repetition rate of 10 kHz is used in the experiment. The laser pulses are transferred into a fiber coupling and collimation system including two FiberPorts (PAF-X-11-A, Thorlabs, New Jersey) and a single-mode fiber, and then expanded twofold through two achromatic lenses with 30 mm (AC254-030-A1, Thorlabs) and 60-mm (AC254-060-A1, Thorlabs) focal length. The expanded laser pulses are directed to an x–y galvanometer scanner (TSH8203M, Century Sunny Technology Co. Ltd., Beijing, China) and focused by a 30-mm focal length objective lens (AC254-030-A1, Thorlabs). The laser irradiation generation and x–y galvanometer scanner are controlled and synchronized by PC1 in Fig. 1 using the scan controlling card (NI6221, National Instrument, Austin). An unfocused ultrasonic transducer (V356, Olympus NDT, Tokyo, Japan; center frequency: 30 MHz) is kept stationary to detect the PA signal. The signal is amplified by two amplifiers (ZFL-500, Mini-Circuits, New York; bandwidth: 0.1 to 500 MHz, gain: 28 dB) and then digitized and recorded by the acquisition card (CompuScope 14200, GAGE, Lockport; sampling rate: 200 MS/s) controlled by PC2 in Fig. 1. The fast photodiode (DET10A, Thorlabs) is used to detect the laser pulses and triggered the acquisition.

We measured the resolution of this experimental system through imaging of gold nanoparticles (diameter <100 nm) solution and calculation of the full-width half-maximum (FWHM) of the Gaussian fitting results.[35] The lateral and axial PA amplitude profiles in Fig. 2 are acquired from the PA response of one nanoparticle. The lateral and axial resolutions are estimated to be 5 and 50 μm according to the FWHM values. The laser pulse energy leaving objective lens is 40 nJ in both resolution measurement and the following experiments.

2.2 *Materials and Measurements*

Fresh abdominal porcine skin tissues are used as scattering biological tissues to cover a phantom light absorber. The phantom is the registered trademark sign [the ® sign in Fig. 3(a)] of a ruler. Each fresh skin is depilated and rinsed briefly with normal saline solution. The skin is cut into $\sim 1 \times 1$ cm^2 squares samples with a mean thickness of 0.5 mm by microtome. Samples are stored in a refrigerator at −70°C for *in vitro* experiment. The anhydrous glycerol is purchased from Tianjin Damao Chemical Reagent Factory, China. Before experiments, glycerol is diluted to different concentrations, i.e., 20%, 40%, and 60% with distilled water. The solutions have a mean refractive index of 1.36, 1.39, and 1.41, respectively.[36] Accordingly, the experiments are divided into groups using 20%, 40%, and 60% glycerol solutions, respectively. Each concentration group consists of four independent experiments. The skin samples are defrosted in physiological saline at room temperature (~25°C) for

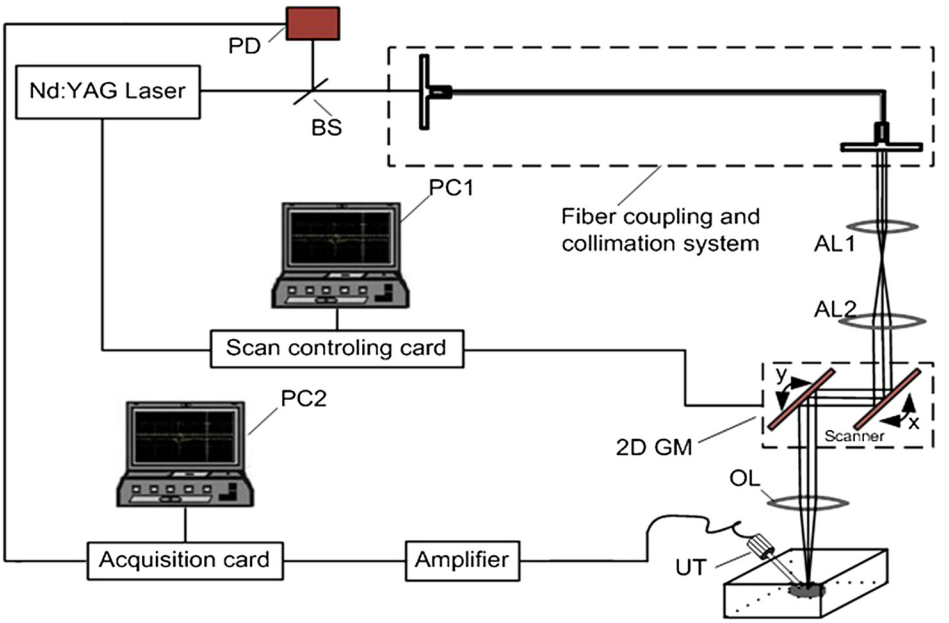

Fig. 1 Schematic of the experimental optical-resolution photoacoustic microscopy (OR-PAM) system. PD: photodiode; BS: Beam splitter; AL1-AL2: achromatic lenses; two-dimensional (2-D) GM: galvanometer; OL: objective lens; PC1-PC2: personal computer UT: ultrasonic transducer.

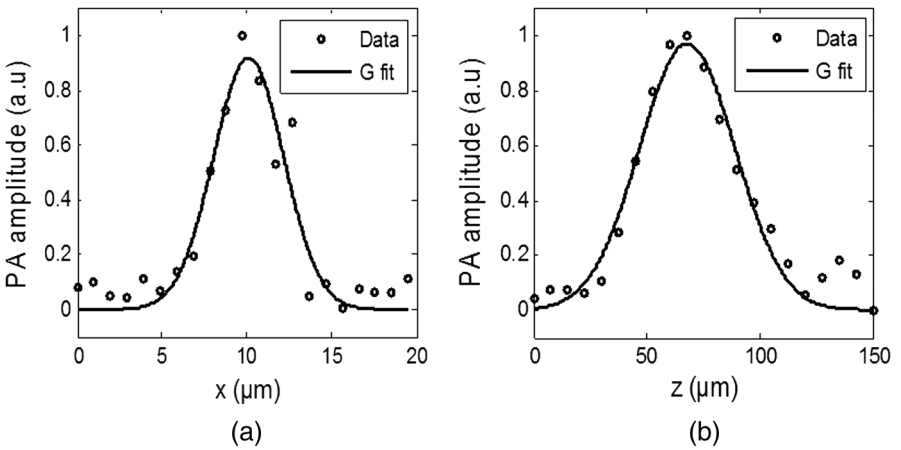

Fig. 2 Resolution of the imaging system by imaging of nanoparticles (diameter < 100 nm). (a) Lateral cross-section profile of a nanoparticle; (b) axial cross-section profile of a nanoparticle.

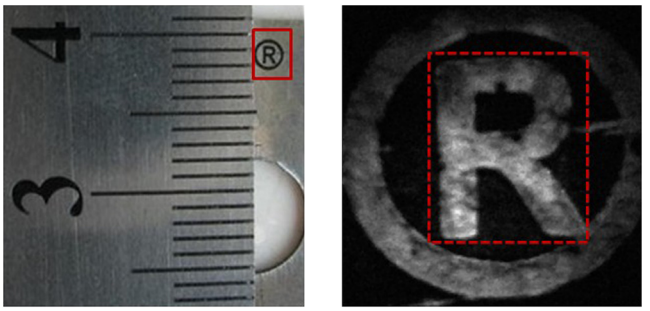

Fig. 3 Photograph of the ruler used and its registered trademark sign (a) and the corresponding 2-D OR-PAM maximum amplitude projection (MAP) image obtained 15 min after application of the 60% glycerol solution. (b) The red solid square in (a) is the registered trademark sign to be imaged. The photoacoustic (PA) signals from the red dotted square area in (b) are statistically analyzed.

~10 min. The register trademark sign is covered by a piece of skin sample and submerged completely in the distilled water and imaged for 3 min to obtain a baseline value using LSOR-PAM. Then, the sign covered with a new skin sample is immersed in the glycerol solution of a certain concentration for 1 h. The PA signals and PAM images are obtained every 15 min during the period for each independent experiments of that concentration group. The procedure is repeated for 20%, 40%, and 60% glycerol solutions. Each skin sample is used only once.

The OCE of each glycerol solution at time intervals 15, 30, 45, and 60 min is evaluated by calculating the enhancement in PA as

$$\mathrm{SEC} = \frac{T_{\mathrm{treated}} - T_{\mathrm{control}}}{T_{\mathrm{control}}}, \tag{1}$$

where T_{control} is the sum of PA signal amplitude in the red dotted square area in Fig. 3(b) obtained at 0 min and T_{treated} is the sum obtained at time interval 15, 30, 45, and 60 min.

3 Results and Discussion

In order to research the OCE of glycerol solutions with different concentrations on the LSOR-PAM imaging modality, the maximum amplitude projection (MAP) images of the registered trademark sign of a ruler covered with the porcine skin tissue are obtained at different time stages. Figure 4 shows photographs of a registered trademark sign covered with a porcine skin tissue under different concentrations of glycerol solution 15 min after the glycerol application, respectively. In Fig. 4, the different OCE is reflected by the visibility of the sign without glycerol as a control, (a) 20% glycerol, (b) 40% glycerol, (c) 60% glycerol, and (d). Visibility differences are mainly due to the hyperosmotic glycerol resulting in refractive index matching between cellular tissue components: cell membrane, cell nucleus, cell organelles, melanin granules, and the extracellular fluid.[11,14] Visibility differences in Figs. 4(b)–4(d) demonstrate that with the increasing of concentration of glycerol, the OCE of skin is dramatically improved. 60% glycerol resulted in the greatest increase of light transmittance and the sign integrality, indicating that more light may be through the skin tissue and

Fig. 4 Photographs of the registered trademark sign covered with a porcine skin tissue under 0%, (a) 20%, (b) 40%, (c) 60%, and (d) glycerol at 15 min, respectively. The black circle is the location of the treatment site of the imaging sign.

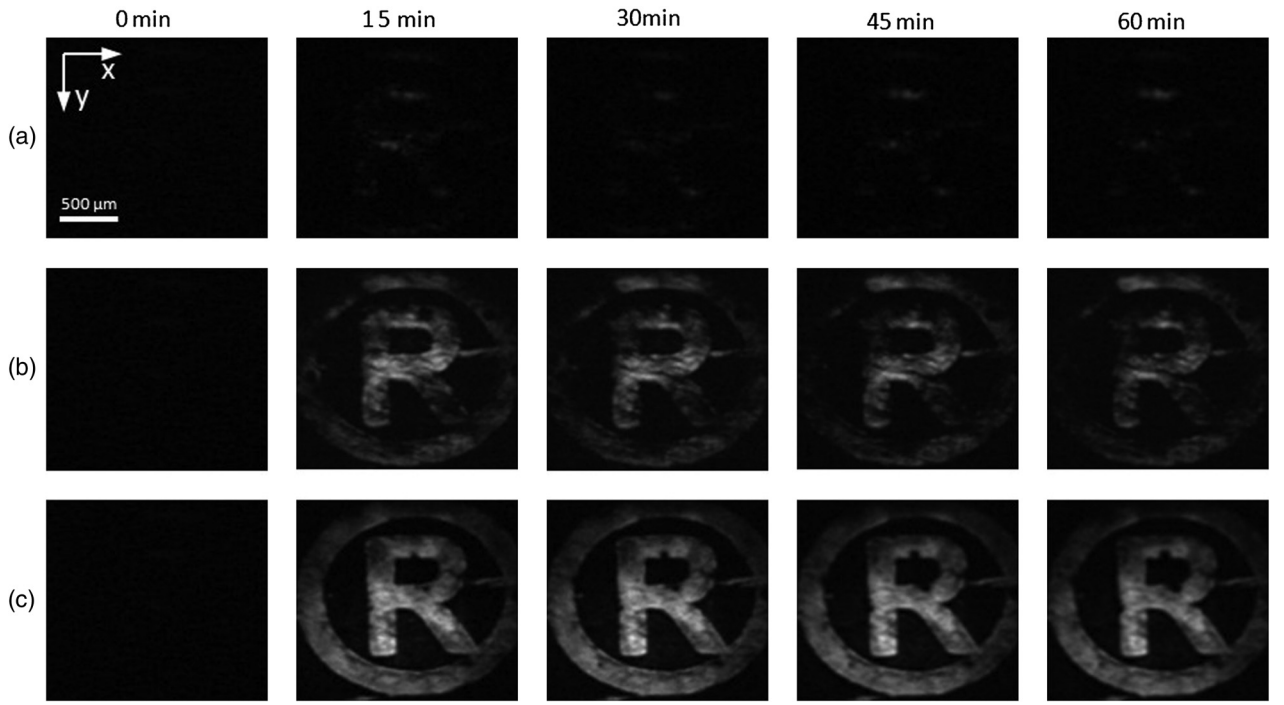

Fig. 5 The OR-PAM MAP images of the sign covered with the skin immersed in glycerol solutions imaged at different time intervals. (a) MAP images with the 20% glycerol (b) MAP images with 40% glycerol. (c) MAP images with 60% glycerol.

delivered into the sign by applying 60% glycerol than others concentrations. The results obtained were similar to these of Mao et al.,[37] who have demonstrated larger optical skin clearing improvement than that with low-concentration glycerol injected into the dorsal dermas of Sprague Dawley (SD) rats from reflectance spectra. Also, Zhong et al.[38] also have proved that the high-concentration solutions induce more transparency of skin than the surroundings tissue. Figure 5 shows the change of LSOR-PAM MAP images of the sign covered with a porcine skin tissue at different time (0, 15, 30, 45, and 60 min) immersed in 20%, 40%, and 60% glycerol solution. Visibility of the sign is improved with the increasing of time and concentration of glycerol in all groups. Still, comparing Figs. 5(a)–5(c), there is a striking difference between each two different concentration groups. The sign becomes slightly clearer after being immersed in 20% glycerol group, but there is still no clearly visible and complete image during the whole process. Meanwhile, the sign is always visible in 40% glycerol group. Moreover,

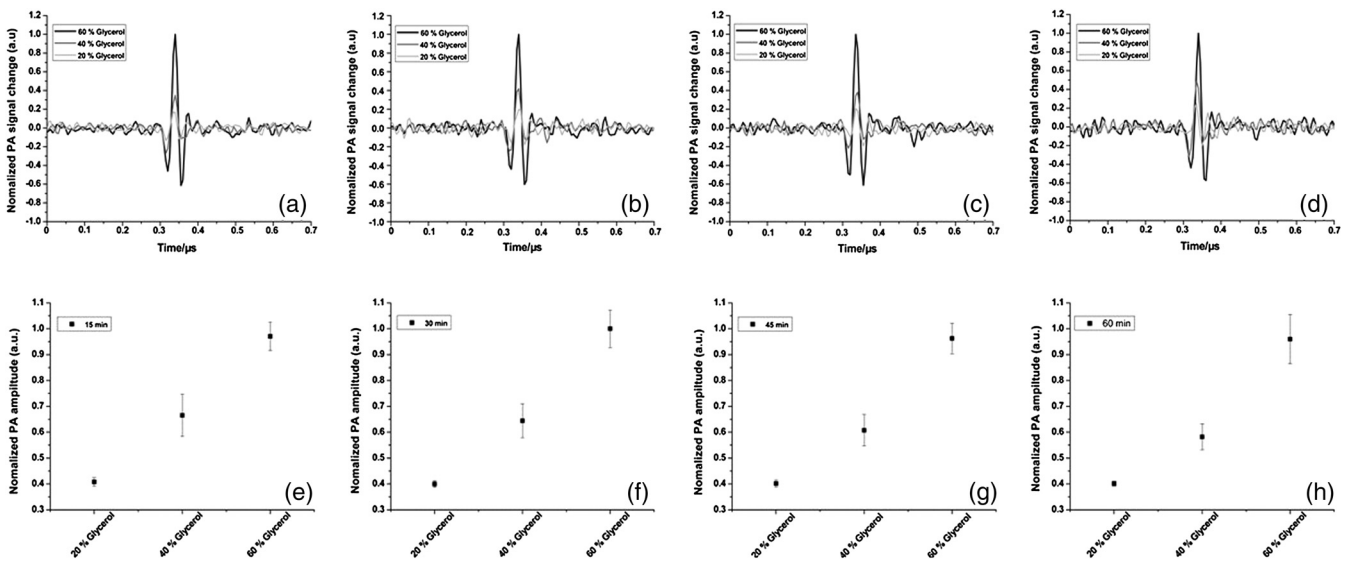

Fig. 6 The normalized PA signal curves and amplitudes changes of the phantom immersed in 20%, 40%, and 60% glycerol at 15 min (a and e), 30 min (b and f), 45 min (c and g), and 60 min (d and h), respectively.

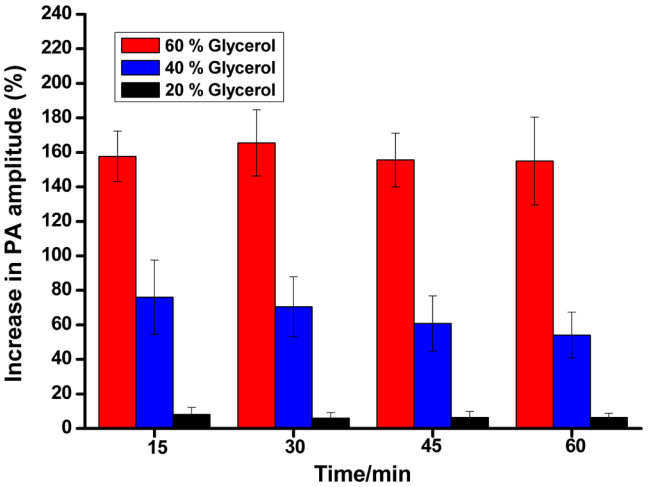

Fig. 7 Dynamic changes of the PA amplitude enhancement after application of 20%, 40%, and 60% glycerol at 0, 15, 30, 45, and 60 min, respectively.

the improvement of sign visibility is extremely prominent in 60% glycerol group as the MAP images are quite clear and complete. The PA signal amplitude changes of different glycerol concentration solutions at time intervals 15, 30, 45, and 60 min are shown in Fig. 6. The better MAP image quality reflects that PA signal amplitude in higher glycerol concentration groups is stronger as can be seen from Fig. 6. The PA signal amplitude can be caused by light penetration differences or ultrasound transmitting change. As higher concentration glycerol solution has higher acoustic attenuation, stronger PA signal amplitude in higher glycerol concentration groups is due to the improved OCE of higher concentration glycerol, which leads to more light penetrating through the skin tissue. A further analysis of the increases of PA signal amplitude is presented in Fig. 7. The result, in Figs. 6(a)–6(h), corresponds to the Fig. 5 results described above. Figure 6 demonstrates that PA signal amplitude increases with the increasing of glycerol concentration at time intervals 15, 30, 45, and 60 min, respectively. From the Fig. 7, we especially observed that PA signal amplitudes of the sign show significant enhancement after applying glycerol solutions with different concentrations gradient. For the low concentration of 20% glycerol, the greatest increase in PA signal amplitude is only 8.1% at 15 min. For the moderate concentration of 40% glycerol, the greatest increase in PA signal amplitude is 76% at 15 min. However, for the high concentration of 60% glycerol, the greatest increase in PA signal amplitude remarkably increases to 165.5% at 30 min, which is 20.4-fold and 2.2-fold to that of 20% and 40% glycerol at 15 min, respectively. As can be seen from Fig. 5, for both 20% and 40% glycerol groups, the visibility of the sign is best at 15 min, whereas for 60% glycerol group, the best is at 30 min. This result corresponds to the Fig. 7 showed above. The difference in the tendency of PA signal amplitude change possibly reflects that high concentrated glycerol solution's diffusion is lower than solutions with a lower concentration. This phenomenon is consistent with previous studies on the relationship of the concentration of aqueous sucrose solution and its diffusion through semi-permeable membranes.[39,40] We believe that the enhancements of PA signal amplitude were mainly caused by the enhancement of the optical penetration due to the reduced scattering coefficient imparted by application of the OCAs and that higher glycerol concentration may result in stronger dehydration effect.[41] The steady-state thermodynamics of water permeation could provide an additional explanation to the behavior of the permeability observed in the study.[39] It is mainly due to that the biological tissues are mostly hypertonic to the applied glycerol–water solution and the water molecules would then spill out of the tissue to reach equilibrium with the concentration gradient between the intercellular space and cell membranes.[42] When the concentration difference is small, such as a dilute solution, the impedance caused by water's flow is not significant and does not greatly affect the flow of glucose.[43]

From the analysis of the aforementioned results, we could conclude that the PAM imaging can be optimized through employing OCA like glycerol. And our results also demonstrate the importance of concentration of OCA to achieve desired OCE on the PAM imaging. In order to provide a more realistic guide for PAM imaging optimization through OTC technology, we would further investigate the OCE of the different kinds and different concentrations of OCA on *in vivo* OR-PAM imaging using animal models. And, it is possible that optical time for PA maximal amplitude is <15 min for the low glycerol concentration, so more researches on studying the real time mutual function mechanism on OR-PAM imaging with OTC technology are necessary. Nonetheless, we for the first time demonstrated that the optical penetration ability and LSOR-PAM imaging depth and contrast could be enhanced by OTC technology. With this technology PAM imaging will have a greater potential for applications in clinical diagnosis and therapy in dermatology.

4 Conclusions

In this study, we investigated the OCE of different concentrations of glycerol solutions in biological tissue on LSOR-PAM imaging. The time-varying and concentration-dependent properties of PA signal amplitude were determined. We have demonstrated a significant improvement of LSOR-PAM imaging performance using tissue OC technique. The PA signal amplitudes and the visibility of a phantom light absorber covered by skin tissues were found to be increasing with the concentration of the glycerol solution. The OCE of the skin tissue caused by OCA could improve the imaging depth and contrast of LSOR-PAM imaging. This result agrees well with studies of the deeply penetrating PAT of biological tissues enhanced with an OCA. Results presented here suggest that this tissue OC method has the potential to become a useful tool for the enhancement of the PAM imaging of biological tissues. And this study may provide a guideline regarding to the use of glycerol for optimal diagnostic and therapeutic effects in dermatology.

Acknowledgments

The research is supported in part by the following grant: National Basic Research Program of China (No. 2011CB707504/3, No. 2010CB933903), National Natural Science Foundation of China (81171377, 61273368), Biomedical Engineering Cross-Research Fund Project of Shanghai Jiao Tong University (YG2011MS45), and Chinese Postdoctoral Science Foundation (2013M531166), Postdoctoral Science Foundation of Shanghai Jiao Tong University (AE606203, 13X100030001).

References

1. S. Hu, K. Maslov, and L. V. Wang, "Noninvasive label-free imaging of microhemodynamics by optical-resolution photoacoustic microscopy," *Opt. Express* **17**(9), 7688–7693 (2009).
2. L. V. Wang and S. Hu, "Photoacoustic tomography: in vivo imaging from organelles to organs," *Science* **335**(6075), 1458–1462 (2012).
3. B. Rao et al., "Hybrid-scanning optical-resolution photoacoustic microscopy for *in vivo* vasculature imaging," *Opt. Lett.* **35**(10), 1521–1523 (2010).
4. S. Hu and L. V. Wang "Photoacoustic imaging and characterization of the microvasculature," *J. Biomed. Opt.* **15**(1), 011101 (2010).
5. G. Ku, K. Maslov, and L. V. Wang, "Photoacoustic microscopy with 2-microm transverse resolution," *J. Biomed. Opt.* **15**(2), 021302 (2010).
6. I. N. Papadopoulos et al., "Optical-resolution photoacoustic microscopy by use of a multimode fiber," *Appl. Phys. Lett.* **102**(21), 211106 (2013).
7. Y. Zhou, J. Yao, and L. V. Wang, "Optical clearing-aided photoacoustic microscopy with enhanced resolution and imaging depth," *Opt. Lett.* **38**(14), 2592–2595 (2013).
8. G. Ku and L. V. Wang, "Deeply penetrating photoacoustic tomography in biological tissues enhanced with an optical contrast agent," *Opt. Lett.* **30**(5), 507–509 (2005).
9. X. D. Wang et al., "Noninvasive photoacoustic angiography of animal brains *in vivo* with near-infrared light and an optical contrast agent," *Opt. Lett.* **29**(7), 730–732 (2004).
10. R. K. Wang, "Signal degradation by coherence tomography multiple scattering in optical of dense tissue: a Monte Carlo study towards optical clearing of biotissues," *Phys. Med. Biol.* **47**(13), 2281–2299 (2002).
11. G. Vargas et al., "Use of an agent to reduce scattering in skin," *Lasers Surg. Med.* **24**(2), 133–141 (1999).
12. V. V. Tuchin, "Tissue optics: light scattering methods and instruments for medical diagnosis," in *SPIE Tutorial Texts in Optical Engineering*, 2nd ed., Vol. TT 38, SPIE Press, Bellingham, Washington (2000).
13. V. V. Tuchin et al., "The coherent, low-coherent and polarized light interaction with tissues undergo the refractive indices matching control," *Proc. SPIE* **3251**, 12–21 (1998).
14. V. V. Tuchin et al., "Light propagation in tissues with controlled optical properties," *J. Biomed. Opt.* **2**(4), 401–417 (1997).
15. V. V. Tuchin et al., "*In vivo* investigation of the immersion-liquid-induced human skin clearing dynamics," *Tech. Phys. Lett.* **27**(6), 489–490 (2001).
16. G. Vargas et al., "Use of osmotically active agents to alter optical properties of tissue: effects on the detected fluorescence signal measured through skin," *Lasers Surg. Med.* **29**(3), 213–220 (2001).
17. I. V. Meglinski et al., "The enhancement of confocal images of tissues at bulk optical immersion," *Laser Phys.* **13**(1), 65–69 (2003).
18. A. N. Bashkatov et al., "*In vivo* investigation of human skin optical clearing and blood microcirculation under the action of glucose solution," *Asian J. Phys.* **15**(1), 1–14 (2006).
19. C. G. Rylander et al., "Dehydration mechanism of optical clearing in tissue," *J. Biomed. Opt.* **11**(4), 041117 (2006).
20. E. A. Genina et al., "Optical clearing of human skin: comparative study of permeability and dehydration of intact and photo-thermally perforated skin," *J. Biomed. Opt.* **13**(2), 021102 (2008).
21. A. N. Bashkatov et al., "*In vivo* and *in vitro* study of control of rat skin optical properties by acting of 40%-glucose solution," *Proc. SPIE* **4241**, 223–230 (2001).
22. A. N. Bashkatov et al., "*In vivo* and *in vitro* study of control of rat skin optical properties by acting of osmotical liquid," *Proc. SPIE* **4224**, 300–311 (2000).
23. A. N. Bashkatov et al., "Study of osmotical liquids diffusion within sclera," *Proc. SPIE* **3908**, 266–276 (2000).
24. V. V. Tuchin, "Controlling of tissue optical properties," *Proc. SPIE* **4001**, 30–53 (2000).
25. Y. Liu et al., "Optical clearing agents improve photoacoustic imaging in the optical diffusive regime," *Opt. Lett.* **38**(20), 4236–4239 (2013).
26. Z. X. Xie et al., "Laser-scanning optical-resolution photoacoustic microscopy," *Opt. Lett.* **34**(12), 1771–1773 (2009).
27. H. F. Zhang, K. Maslov, and L. V. Wang, "*In vivo* imaging of subcutaneous structures using functional photoacoustic microscopy," *Nat. Protoc.* **2**(4), 797–804 (2007).
28. H. F. Zhang et al., "Functional photoacoustic microscopy for high-resolution and noninvasive *in vivo* imaging," *Nat. Biotechnol.* **24**(7), 848–851 (2006).
29. K. Maslov et al., "Optical-resolution photoacoustic microscopy for *in vivo* imaging of single capillaries," *Opt. Lett.* **33**(9), 929–931 (2008).
30. B. Choi et al., "Determination of chemical agent optical clearing potential using *in vitro* human skin," *Lasers Surg. Med.* **36**(2), 72–75 (2005).
31. X. Xu, Q. Zhu, and C. Sun, "Combined effect of ultrasound-SLS on skin optical clearing," *IEEE Photonics Technol. Lett.* **20**(24), 2117–2119 (2008).
32. N. A. Trunina, V. V. Lychagov, and V. V. Tuchin, "OCT monitoring of diffusion of water and glycerol through tooth dentine in different geometry of wetting," *Proc. SPIE* **7563**, 75630U (2010).
33. G. Vargas et al., "Morphological changes in blood vessels produced by hyperosmotic agents and measured by optical coherence tomography," *Photochem. Photobiol.* **77**(5), 541–549 (2003).
34. D. Zhu, H. Cui, and Z. Mao, "Transient response and hysteresis of blood vessel in chick chorioallantoic membrane by hyperosmotic agents," *J. Biomed. Opt.* **13**(2), 021106 (2008).
35. S. Q. Ye et al., "Label-free imaging of zebrafish larvae *in vivo* by photoacoustic microscopy," *Biomed. Opt. Express* **3**(2), 360–365 (2012).
36. R. K. Wang et al., "Concurrent enhancement of imaging depth and contrast for optical coherence tomography by hyperosmotic agents," *J. Opt. Soc. Am. B.* **18**(7), 948–953 (2001).
37. Z. Z. Mao et al., "Influence of glycerol with different concentration on skin optical clearing and morphological changes *in vivo*," *Proc. SPIE* **7278**, 72781T (2008).
38. H. Q. Zhong et al., "*In vitro* study of ultrasound and different-concentration glycerol-induced changes in human skin optical attenuation assessed with optical coherence tomography," *J. Biomed. Opt.* **15**(3), 036012 (2010).
39. P. N. Henrion, "Diffusion in the sucrose + water system," *Trans. Faraday Soc.* **60**, 72–74 (1964).
40. L. G. Longsworth, "Diffusion measurements, at 25, of aqueous solutions of amino acids, peptides and sugars," *J. Am. Chem. Soc.* **75**(22), 5705–5709 (1953).
41. Y. A. Menyaev et al., "Optical clearing in photoacoustic flow cytometry," *Biomed. Opt. Express* **4**(12), 3030–3041 (2013).
42. A. Kotyk and K. Janáček, "*Membrane Transport: An Interdisciplinary Approach*, Plenum Press, New York (1977).
43. M. G. Ghosn et al., "The effect of solutions' concentration on diffusion in scleral tissues," *Proc. SPIE* **6791**, 679107 (2008).

Qingliang Zhao received his MS degree in MOE Key Laboratory of Laser Life Science & Institute of Laser Life Science and College of Biophotonics from South China Normal University, China, in 2011. He is currently a PhD candidate at School of Biomedical Engineering, Shanghai Jiao Tong University. His research interest is mainly focused on the development of optical coherence tomography, tissue optical clearing technology and photoacoustic microscopy technologies for imaging of biological tissue.

Lin Li received his B.S. degree in biomedical engineering from Dalian University of Technology (DUT), Dalian, China, in 2011. He is currently a PhD candidate in the School of Biomedical Engineering, Shanghai Jiao Tong University.

Xia Jiang received the BS degree in clinical medical department from NanJing University, China, in 1999, and the ME degree in the department of internal medicine of Hua Shan Hospital from Fudan University, China, in 2002, and the PhD degree in biomedical engineering from Shanghai Jiao Tong University, China, in 2012. She is currently a postdoctor at Shanghai Jiao Tong University. Her research interests include laser-tissue interaction, biomedical applications of lasers and electrooptics.

Qiushi Ren is a PKU-COE endowed chair professor, MOE Chang-Jiang distinguished professor chairman in the Department of Biomedical Engineering, Peking University, China. His research mainly focuses on laser-tissue interaction, ophthalmology and visual science and molecular imaging, minimal invasive surgeries, and neural engineering.

Xinyu Chai is a professor of School of Biomedical Engineering, Shanghai Jiao Tong University, China. He received his PhD degree in biomedical engineering from Xi'an Jiaotong University in 1998. Currently he is a full professor in the School of Biomedical Engineering of the SJTU. He is a member of the editorial board of *Interdisciplinary Sciences* and the reviewer of *Artificial Organs*, a member of ARVO and SPIE.

Chuanqing Zhou obtained his PhD degree in biomedical engineering from Shanghai Jiao Tong University in 2007. He is currently an associate professor in the School of Biomedical Engineering, Shanghai Jiao Tong University, China. His research interests focus on visual optics, ophthalmology and biomedical optical imaging.

Qian Li: biography is not available.